NASA CR - 132414

EVALUATION OF GRAPHITE COMPOSITE MATERIALS FOR BEARINGLESS HELICOPTER ROTOR APPLICATION

by

M. G. Ulitchny and J. J. Lucas

Prepared under Contract No. NASI-12622

by

Sikorsky Aircraft,

Division of United Aircraft Corporation,

Stratford, Conn.

January 1974

for

NATIONAL AERONAUTICS AND SPACE ADMINISTRATION

NASA CR - 132414

EVALUATION OF GRAPHITE COMPOSITE MATERIALS FOR BEARINGLESS HELICOPTER ROTOR APPLICATION

by

M. G. Ulitchny and J. J. Lucas

Prepared under Contract No. NASI-12622

by

Sikorsky Aircraft,

Division of United Aircraft Corporation,

Stratford, Conn.

January 1974

for

NATIONAL AERONAUTICS AND SPACE ADMINISTRATION

FORWARD

This report was prepared by Sikorsky Aircraft, Division of United Aircraft Corporation, under NASA Contract NAS1-12622 and covers the work performed during the period August 1973 to December 1973.

UNITS

Dimensional information is presented in the U.S. customary system based on the foot, pound, second system. The equivalent values in the International System of Units (SI) are shown in parentheses. An exception is made for figures which refer to test specimens, the dimensions of which are given in inches only. All calculations were performed in the customary system and converted to the SI units.

CONTENTS

LIST OF ILLUSTRATIONS

LIST OF ILLUSTRATIONS

LIST OF TABLES

EVALUATION OF GRAPHITE COMPOSITE MATERIALS FOR BEARINGLESS HELICOPTER ROTOR APPLICATION*

by

M. G. Ulitchny and J. J. Lucas
Sikorsky Aircraft
Division of United Aircraft
Stratford, Connecticut

SUMMARY

Small scale combined load fatigue tests were conducted on twelve unidirectional graphite-glass scrim-epoxy composite specimens. The specimens were 1 in. (2.54 cm) wide by 0.1 in. (.25 cm) thick by 5 in. (12.70 cm) long. The fatigue data was developed for the preliminary design of the spar for a bearingless helicopter main rotor. Three loading conditions were tested. Combinations of steady axial, vibratory torsion, and vibratory bending stresses were chosen to simulate the calculated stresses which exist at the root and at the outboard end of the pitch change section of the spar. Calculated loads for 150 knots (77.1 m/sec) level flight were chosen as the baseline condition. Test stresses were varied up to 4.4 times the baseline stress levels. Fatigue damage resulted in reduced stiffness; however, in no case was complete fracture of the specimen experienced. At stress levels three times higher than level flight stresses, a 5 to 12 percent reduction in the torsional modulus and a 3 to 6 percent reduction in the flexural modulus occurred. At higher stress levels, 3.5 to 4.4 times level flight stresses, reductions in torsional modulus up to 75 percent and reductions in flexural modulus up to 20 percent accompanied by matrix cracking occurred.

Damping and natural frequency measurements showed that a significant increase in damping and a reduction in natural frequency occurred only in specimens where matrix cracking was detected. Significant and meaningful changes in damping could not be detected in those specimens which exhibited torsional modulus changes of less than about 15 percent and where no internal matrix cracking was evident.

---

*The contract research effort which has lead to the results in this report was financially supported by USAAMRDL (Langley Directorate).

Natural and artificial weathering was initiated on a total of twelve specimens. The six natural weathered specimens exhibited essentially no change in surface condition, after 143 days exposure. The six artificial weathered specimens exhibited considerable resin leaching on the scrim ply face and a loss in weight of about one-half percent as a result of the resin loss after 600 hours exposure on each face (equivalent to two years of Florida exposure).

SECTION 1.0 INTRODUCTION

The cross-beam bearingless main rotor concept takes advantage of the anisotropic properties of composites to provide significant improvements in maintainability, reliability, and structural efficiency by eliminating critical bearings in the hub and in the pitch control mechanism. A schematic diagram of a cross-beam main rotor system is shown in Figure 1. In this concept, and in common with other hingeless rotor systems, blade flapping and in-plane motions are accommodated by flexure of the spar. However, unlike other blade systems, blade pitch is achieved by elastically twisting the spar. The result is a simple bearingless rotor system. Composite materials provide the necessary axial strength and flexural stiffness for the spar without high torsional rigidity which would result in high pitch link loads. Since bearings are not necessary for normal flight motions, the composite spars can be continuous through the hub to react centrifugal loads efficiently.

With the cross beam rotor system, lead-lag, flapping and feathering bearings are eliminated, and this results in a simple bearingless rotor system. The net result is a compounding of weight saving from the application of light weight composites and the elimination of bearings and bearing support structures. The combination shows promise of achieving a 40 percent weight saving and 50 percent reduction in life cycle cost, because of the simplicity of design and elimination of parts. Structural loadings are well within the capabilities of the present state of the art of advanced high strength composites.

An 11 foot (3.35 m) diameter bearingless cross-beam type tail rotor has been successfully developed and flight tested by Sikorsky Aircraft. In addition, a 62 foot (18.9 m) diameter demonstrator main rotor of the cross-beam type has been tested on an 8000 horsepower (59.6×10^5 watt) test stand. This demonstrator rotor was built up from steel and boron-epoxy using standard components. It was designed to be aerodynamically and aeroelastically similar to an all composite construction. The results of these tests will be used to advance the preliminary design of an all composite rotor system. United Aircraft Research Laboratory is conducting a theoretical study of a cross-beam main rotor design under NASA Contract NAS1-10960, Reference (a). This work includes wind tunnel experiments on a sub scale rotor to determine control and blade loadings as well as aeroelastic stability. Thus at the present time the feasibility of developing a bearingless cross-beam main rotor has been demonstrated but structurally sound design configuration of the critical details of an all composite rotor have not been developed.

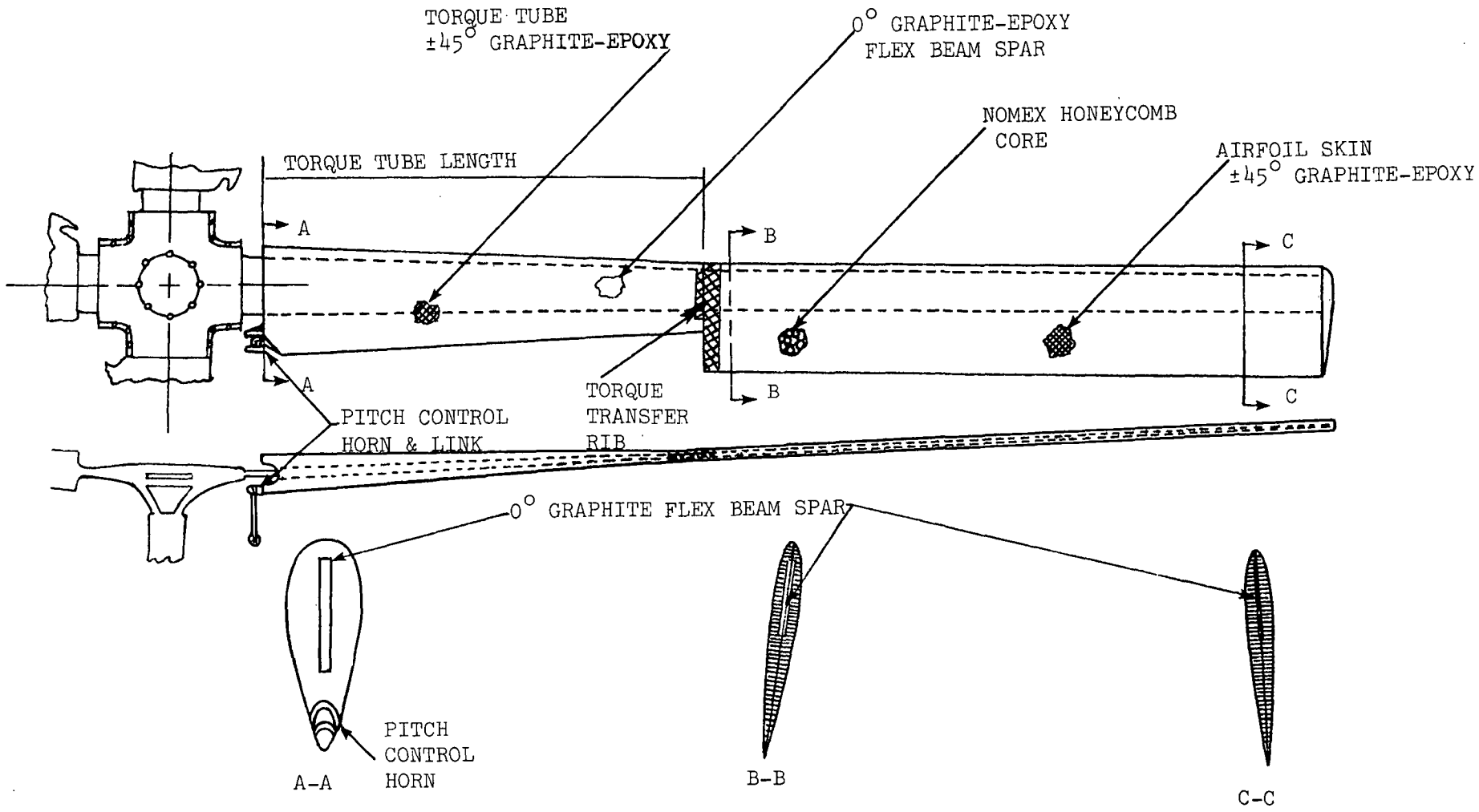

FIGURE 1. BEARINGLESS ROTOR CONFIGURATION PROVIDES 40% WEIGHT SAVINGS.

The purpose of this investigation was to provide fatigue data for unidirectional graphite-glass scrim-epoxy composites under loading conditions which simulate those encountered by a helicopter main rotor. The fatigue data thus generated will be used to aid in the preliminary design of a full size bearingless, composite main rotor.

SECTION 2.0 MATERIALS, EQUIPMENT AND PROCEDURES

2.1 MATERIALS AND TEST SPECIMEN DESIGN

The material used for test specimens in this program was Hercules, Inc. type A/S graphite fiber with type 104 woven glass scrim prepreged by Dexter Materials Corp. with DM-101 resin. This resin is a 275°F (135°C) curing, modified epoxy system designed for structural applications that require operation at temperatures up to 200°F (92°C). Certification tests were performed on this material for comparison to the requirements of Sikorsky Standard SS-9611, Reference (b). The results of the certification tests and the requirements of Reference (b) are shown in Table I. Although there were minor differences between the actual properties and the requirements of the specification, they were not considered to be significant.

A single 10 ply panel, approximately 12 in. (30.5 cm) x 24 inches (61 cm), was laid up from 12 inch (30.5 cm) wide tape. The panel was vacuum bagged and autoclave cured at 100 psi (6.9×10^5 n/m^2) plus vacuum for 2 hours at 275°F (135°C). A nominal as cured thickness of 0.010 inches (0.025 cm) per ply was obtained, 0.009 inches (0.023 cm) graphite and 0.001 inches (0.002 cm) glass scrim. After the panel was cured, unidirectional fiberglass doublers were bonded to each end of that portion of the panel to be made into fatigue test specimens in such a manner that the fiber direction of both the graphite test specimens and the fiberglass doublers was parallel to the long dimension of the specimen. Twelve fatigue test specimens were cut from the panel using a diamond saw. These specimens were then ground to final width, and the doublers to final thickness to assure smooth, parallel edges. A drill jig was used to align and drill the holes prior to bolting steel cuffs at each end of the specimen. The cuffs are designed so that load transfer from cuffs to specimens is by a combination of friction and pin bearing. Figure 2 shows the details of the specimens used for the fatigue tests.

No doublers were bonded to the twelve weathered specimens because any measured weight gain or loss due to such doublers would not be distinguishable from that due to the actual graphite-epoxy specimens. When the weathered specimens are tested, doublers will be bonded with room temperature curing adhesive.

TABLE I

REQUIREMENTS OF SS-9611 AND CERTIFIED TEST RESULTS
FOR TYPE A/S GRAPHITE COMPOSITE MATERIALS

Property	SS-9611 Requirement	Certified Test Results from DMC*	
Resin Content	44 ± 3%	44.7%	
Volatile Content	1.0% Max.	0.2%	
Horizontal Shear At	PSI (Min.)**	$(n/m^2 x 10^6)$	PSI(Min.)** $(n/m^2 x 10^6)$
-67°F (55°C)	Room Temp. Value ±5%	13,800	95,137
70°F (21°C)	12,000 82.7	12,100	83,417
160°F (71°C)	≥95% of Room Temp.Value	11,700	80,660
250°F (121°C)	≥75% of Room Temp.Value	9,360	64,528
Longitudinal Flexural Strength At	PSI (Min.)**	$(n/m^2 x 10^6)$	PSI(Min.)** $(n/m^2 x 10^6)$
-67°F (55°C)	Room Temp. Value ±5%	198,200	1,366
70°F (21°C)	200,000 1,378	208,200	1,438
160°F (71°C)	≥95% of Room Temp.Value	222,400	1,533
250°F (121°C)	≥75% of Room Temp.Value	193,500	1,333
Longitudinal Flexural Modulus At	PSI ±6%	$(n/m^2 x 10^9)$	PSI $(n/m^2 x 10^9)$
-67°F (55°C)	Room Temp. Value ±5%	$16.2 x 10^6$	111.7
70°F (21°C)	$16.2 x 10^6$ 111.7	$16.2 x 10^6$	111.7
160°F (71°C)	≥95% of Room Temp.Value	$17.3 x 10^6$	119.3
250°F (121°C)	≥75% of Room Temp.Value	$15.7 x 10^6$	108.2
		gm/sq ft	gm/sq m.
Graphite Fiber Weight	Must Be Reported	19.46	209
Glass Fiber Weight	Must Be Reported	1.88	20.2

*Information Furnished by Dexter Materials Corporation

**Average of Five Test Specimens

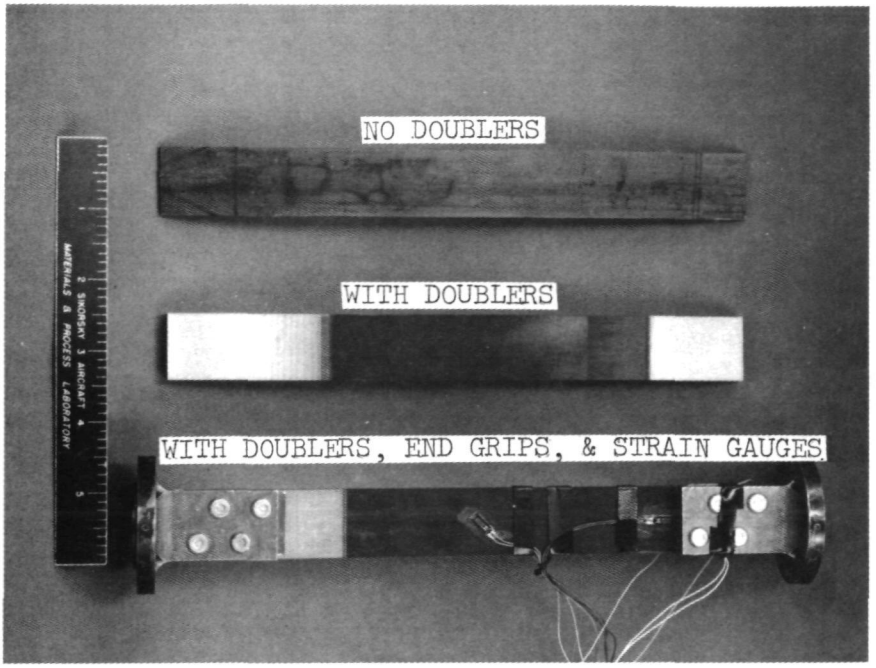

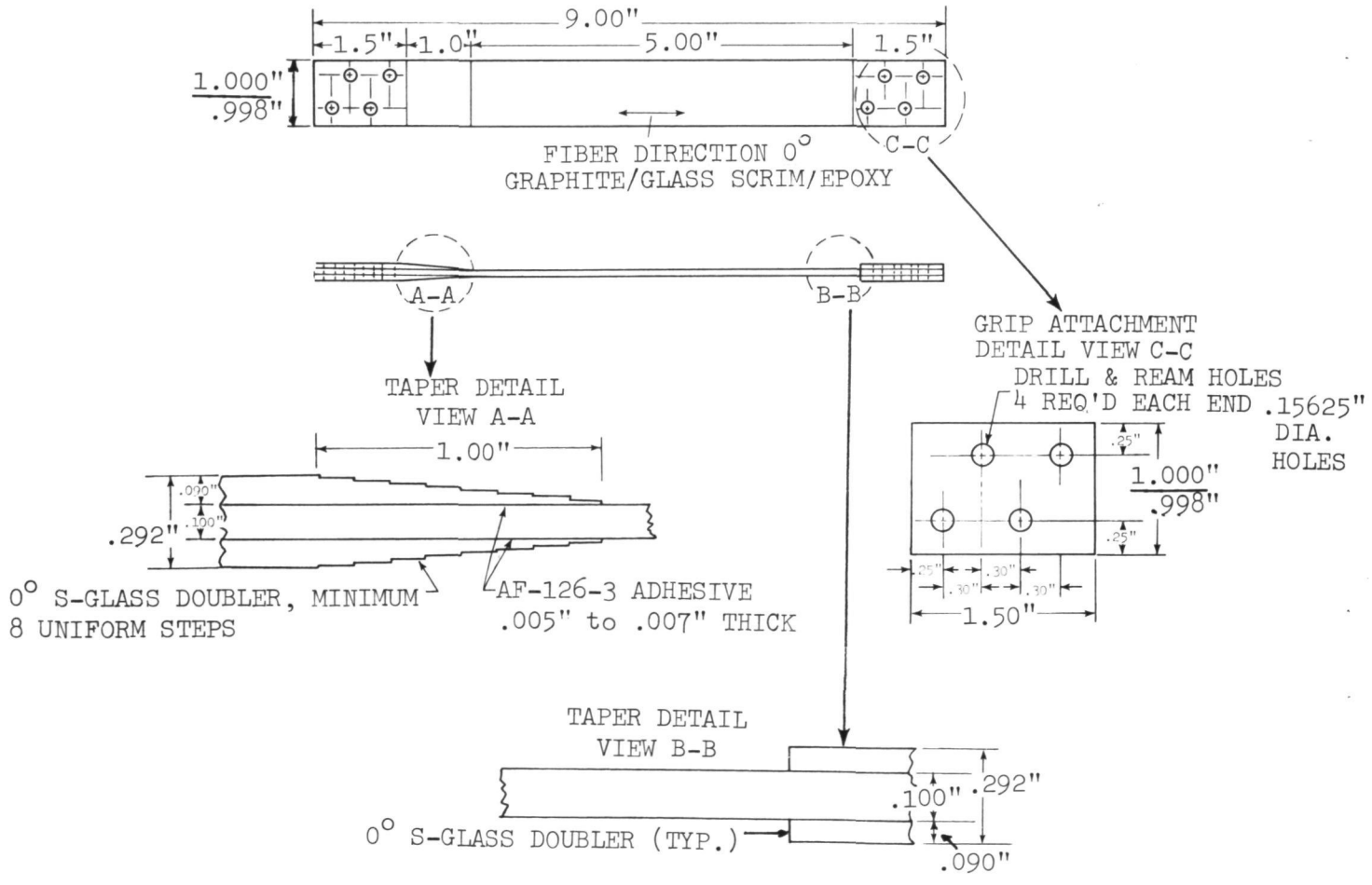

FIGURE 2. PROVEN FATIGUE SPECIMEN DESIGN FOR MATERIALS TESTS.

2.2 EQUIPMENT AND PROCEDURES

2.2.1 Modulus, Damping and Frequency Calibrations

Strain gauges were attached to all specimens to detect flatwise bending, edgewise bending, and torsion. Specimens with end grips and strain gauges in place are shown in Figure 2. The edgewise and flatwise bending gauges were placed at the end of the specimen which experienced the highest bending loads. Separate tests showed that the bending stress levels at the low stress end were about 10 percent of the maximum value. However, the ratio of flatwise to edgewise stress was nearly constant along the length of the specimen. The torsional gauges were placed in the middle of the gauge length of the specimen to avoid end effects in measuring torsional strains.

Torsional modulus was determined using the test fixture shown in Figure 3. Known torques were applied to the specimen and the outputs for the torsion strain gauges were used to calculate a torsional modulus for each specimen. In addition, the angle of twist for each applied torque was recorded. Changes in the angle of twist as a function of fatigue cycles were used to measure the percentage change in torsional modulus.

Flexural modulus was determined using the test fixture shown in Figure 4. The specimen was loaded as a cantilever beam and the outputs of the bending strain gauges were recorded. This was done for pure flatwise and pure edgewise bending on each specimen. The average of the moduli calculated for edgewise and flatwise bending was used as the flexural modulus. As with the torsional measurements, the deflection for a given applied load was measured. Specimen strain gauge outputs were monitored using a strain gauge bridge, amplifier, and oscilloscope. During testing, specimen stresses were adjusted until they were within three percent of the desired values.

Changes in flexural modulus, as a function of fatigue cycles, determined by measuring changes in edgewise deflection were approximately the same as those determined by flatwise deflection measurements. However, since the edgewise deflections were only about one-fifth to one-fourth of the flatwise deflections for a given stress, the precision of the measurements was better in the flatwise direction. Thus, changes in flatwise deflection were used exclusively to determine the effect of fatigue cycles on flexural modulus.

Damping and natural frequency measurements were made on the apparatus shown in Figure 5. The specimen was set up as a flexure pendulum with an accelerometer attached to the free end. The specimen was set into oscillation and the amplitude allowed to diminish in free decay. The output of the acceler-

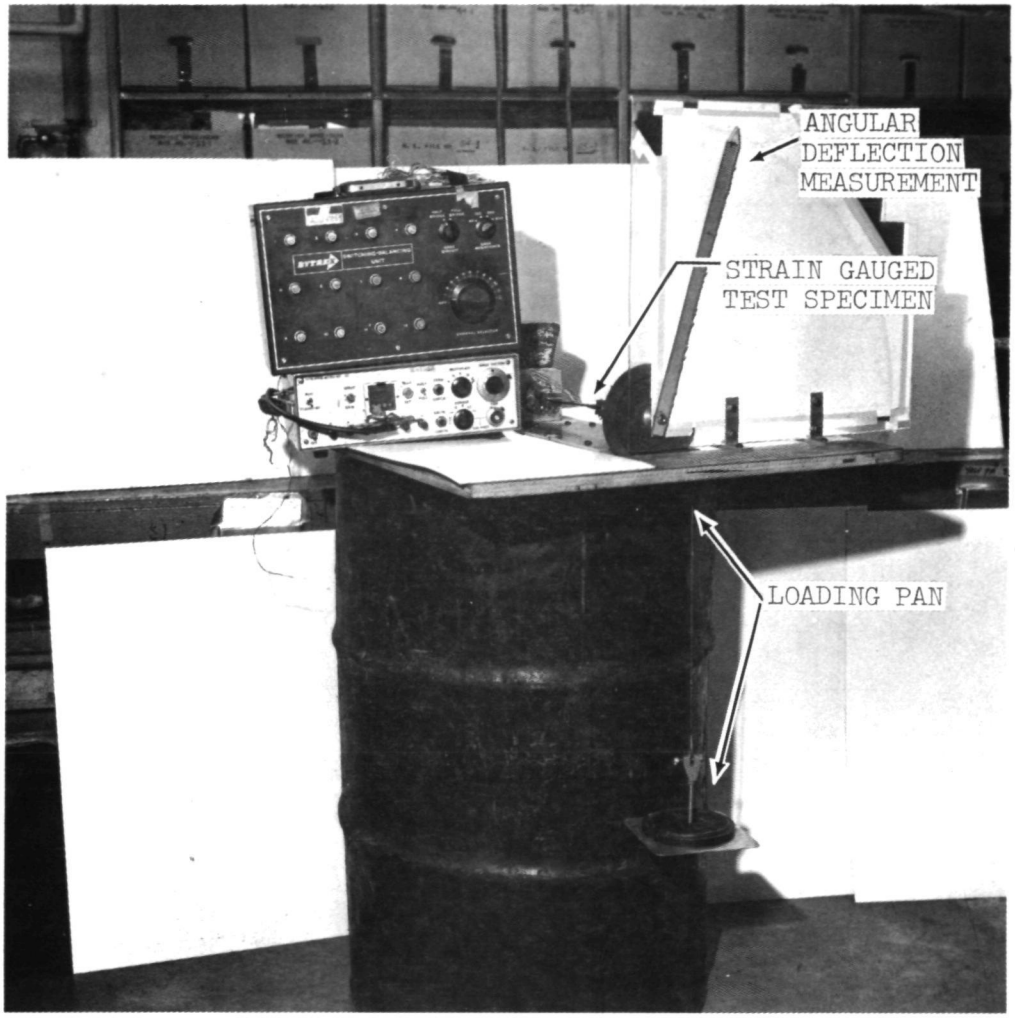

FIGURE 3. TORSIONAL MODULUS AND STIFFNESS MEASURED STATICALLY.

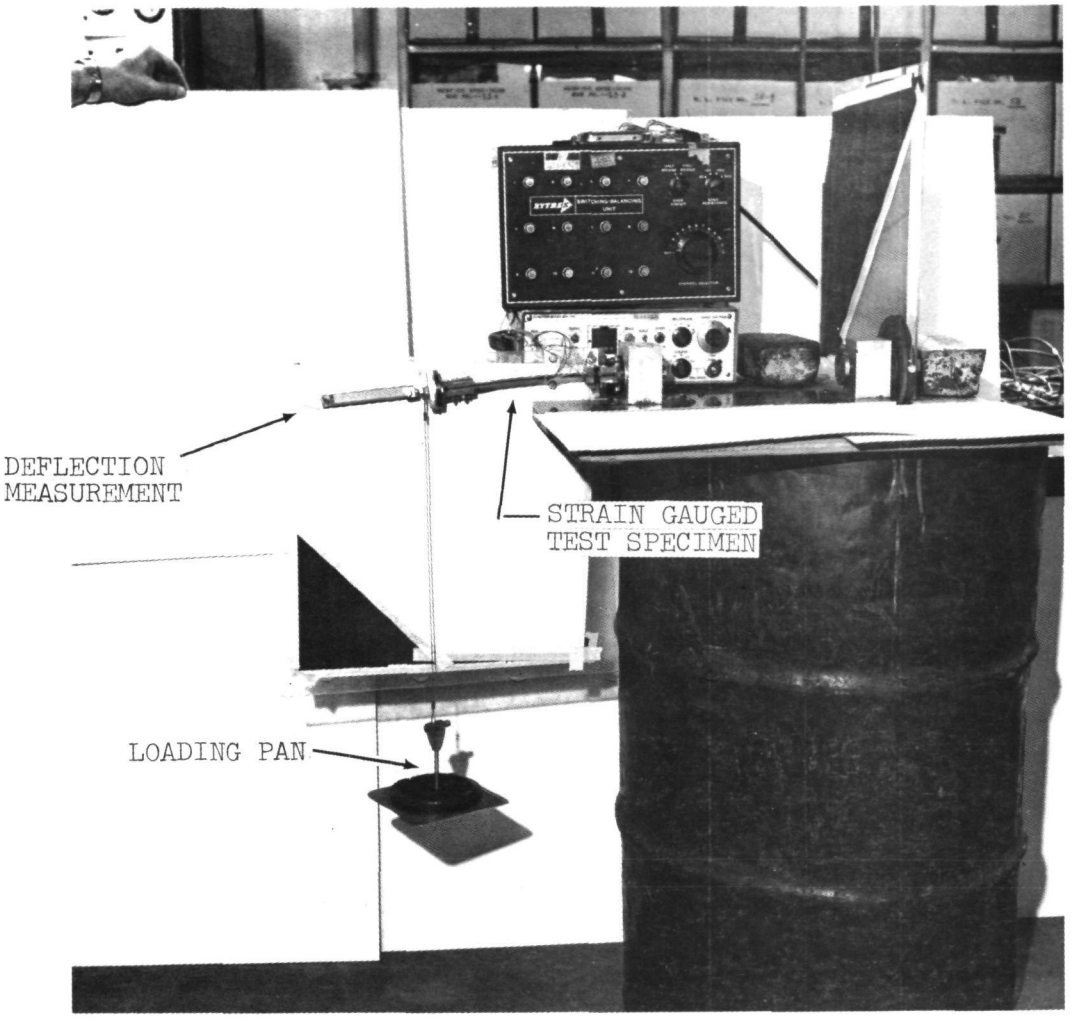

FIGURE 4. FLEXURAL MODULUS AND STIFFNESS MEASURED STATICALLY.

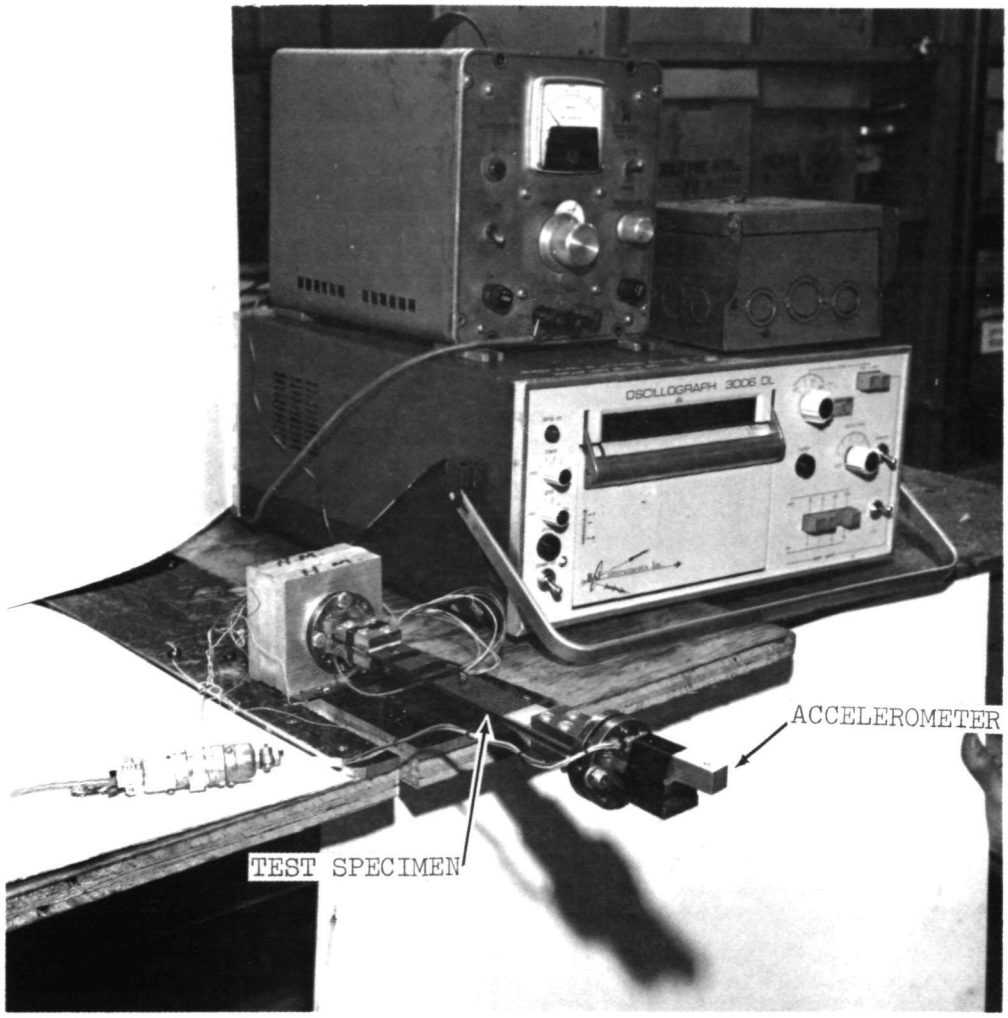

FIGURE 5. DAMPING AND NATURAL FREQUENCY WAS MEASURED PERIODICALLY.

ometer was recorded using an oscillograph recorder. A reference signal was also recorded so that the natural frequency of the specimen could be accurately measured. The decay of natural frequency as a function of cycles was used to calculate the ratio of damping capacity, C, to critical damping capacity, C_c.

The static measurements of displacement for known torques and bending loads as well as damping and frequency measurements were made at 0, 10^6, 5×10^6 and 10^7 fatigue cycles. By this means the effect of fatigue cycles on the torsional and bending moduli as well as the damping characteristics were monitored.

Figure 6 shows the load cells built into the machine which were to be used to continuously monitor torsional load. The output of these load cells was so small that no meaningful data could be obtained. For this reason continuous torsional load data was not obtained.

2.2.2 Combined Load Fatigue Tests

A unique combined load fatigue machine designed and built by Sikorsky Aircraft was used to conduct tests under various combinations of steady axial, vibratory bending, and vibratory torsional loads. Details of this machine are shown in Figure 7. Two bending eccentrics, seen in Figure 7, are used to apply the bending load. The offset of each eccentric can be varied to control not only the maximum amplitude of the bending stress but also the bending stress distribution along the length of the specimen.

The ratio of flatwise bending stress to edgewise bending stress is controlled by adjusting the angle of the plane of the specimen with respect to the bending plane on the machine. For example, if the angle between the plane of the specimen and the bending plane of the machine is 90 degrees, then the applied bending load is pure flatwise. If this angle is varied from 90 degrees increasing amounts of edgewise bending are introduced until the bending becomes pure edgewise at an angle of 0 or 180 degrees.

The third eccentric seen in Figure 7 controls the torsional stress on the specimen. The three eccentrics are connected by timing belts in such a manner that maximum bending and maximum torsional stresses occur simultaneously. This arrangement best simulates cyclic torsional and bending stresses experienced by the actual rotor blade.

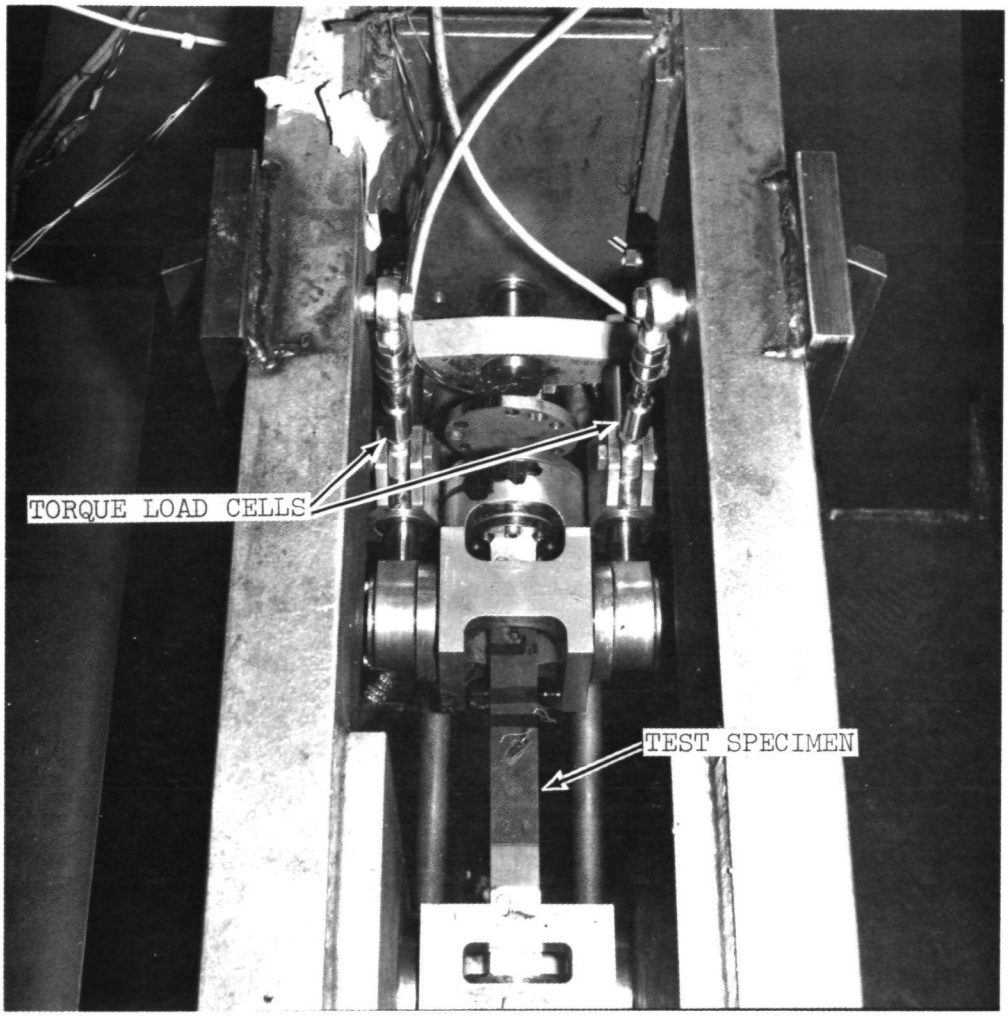

FIGURE 6. COMBINED LOAD MACHINE SHOWING TORQUE LOAD CELLS.

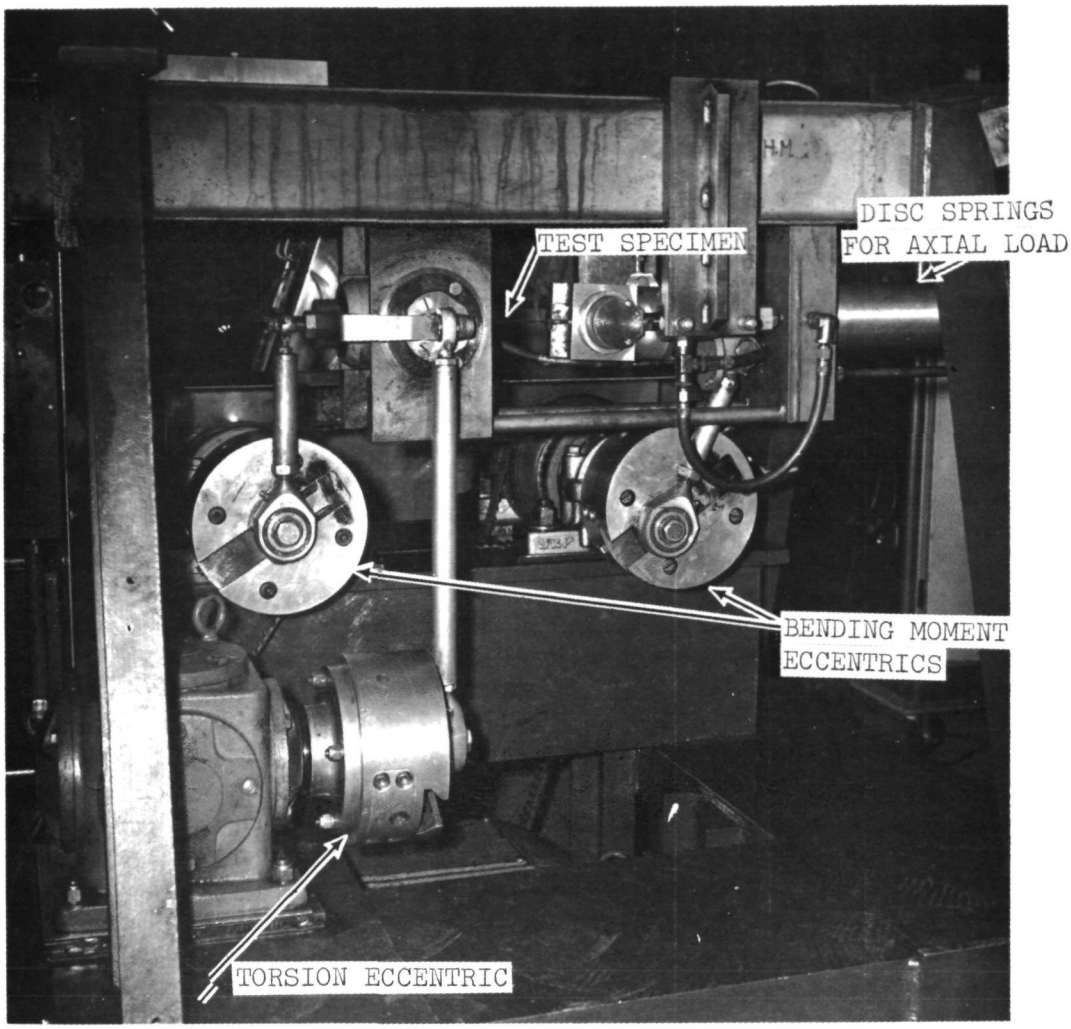

FIGURE 7. SIKORSKY'S UNIQUE COMBINED LOAD FATIGUE TEST FACILITY.

The steady axial load simulating centrifugal force is applied by disk springs. Since these springs are "soft" they can accommodate the small changes in specimen length which take place during the fatigue cycle without appreciably changing the axial stress.

2.2.3 Test Conditions

The test conditions were based on predictions of the stress conditions that occur in a full scale bearingless composite main rotor that uses the aeroelastic characteristics of the Sikorsky Aircraft 62 ft. (18.9 m) diameter demonstrator rotor. The demonstrator rotor has been whirl tested and a reasonable aeroelastic data basis has been established for predicting the all composite full scale rotor loading.

All test conditions were developed for the flex section of the blade spar (see Figure 1) for a flight condition of 150 knots (77.1 m/sec) at a gross weight of 18,000 lbs. (8165 kgm). This flex section exists approximately between Station 25 and Station 115 of the spar (stations are in inches). At this early stage of analysis the exact geometry of the flex section in not known, such geometry will be controlled by the material design allowables to be defined by this program. Using the bending moments and pitch angles determined experimentally from the 62 ft. (18.9 m) diameter demonstration rotor, a preliminary sizing of the all composite spar flex section was determined. This sizing was necessary to establish the types of failure modes and critical margin of safety required on an all composite blade. Examination of the expected stresses on the flex beam show that the critical locations on the beam are the inboard and outboard stations.

The first fatigue test condition was based on the inboard cross section stress state which is controlled by high spar bending stresses with a moderate amount of vibratory shear stress. At this inboard station the stress state is dominated by the root bending moments, vibratory shear stresses are low because the outboard station, which has a smaller cross sectional area, must support the same torsional loads.

The second fatigue test condition addressed the problem of high torsional stresses which occur at the outboard station of the flex beam. Bending stresses at the outboard station are lower than at the root end station. However, the centrifugal stress is higher for the outboard station due to the smaller cross section. The third test condition was designed to determine the sensitivity to centrifugal stresses. The third condition duplicated the flexural and torsional stresses of condition 2 but the steady centrifugal stress was increased by 100 percent from 8000 psi (55.2×10^6 n/m^2) to 16,000 psi

(110.3 x 10^6 n/m^2). Table II gives the baseline, i.e., 150 knot (77.1 m/sec) level flight 18,000 lbs (8165 kgm) gross weight, stresses which were calculated for each of the test conditions.

During fatigue testing the vibratory bending and torsional loads were increased by a constant percentage above the calculated flight stresses shown in Table II. Thus the ratios of flatwise to edgewise bending and the ratio of flatwise bending to torsion were constant for any test condition. The axial stress remained constant, for a given test condition, and was not increased above calculated flight stress levels. The bending and torsional stresses were increased from 2.2 to 4.4 times calculated level flight stresses as discussed in more detail in subsequent sections of this report.

2.2.4 Weathering

Specimens for natural weathering were weighed, measured, and placed on the roof of the Stratford, Connecticut plant of Sikorsky Aircraft. A fixture was made which holds these specimens at a 45 degree angle to the horizontal facing south, Figure 8. These specimens are in a completely exposed location unprotected from sunlight and rain by any nearby structures. Specimens to be weathered artifically were placed in an Atlas Electric Devices Co. Model XW Weatherometer. Since only one face of the specimens could be exposed at a time they were turned to expose the opposite face after each 300 hour exposure period. A 300 hour exposure in the Weatherometer is equivalent to one year in a Florida environment.

TABLE II

CALCULATED SPAR STRESSES FOR 150 KNOTS (77.1 m/sec), 18,000 LBS. (8165 kgm) GROSS WEIGHT LEVEL FLIGHT

Condition	Location	Stresses				Stress Ratios	
		Flatwise Bending ± PSI ($\bar{n}/m^2 x 10^6$)	Edgewise Bending ± PSI ($\bar{n}/m^2 x 10^6$)	Torsion Shear ± PSI ($\bar{n}/m^2 x 10^6$)	Axial PSI ($n/m^2 x 10^6$)	Flatwise/Edgewise $\sigma F/\sigma E$	Flatwise/Torsion $\sigma F/\tau$
1. High Bendirg Moderate Torsion Low Axial	Flex Beam Root	17,000 (117.1)	5,000 (34.4)	1,100 (7.5)	4,000 (27.5)	3.4/1	15.4/1
2. Low Bending High Torsion Moderate Axial	Flex Beam Outboard Station	6,800 (46.8)	2,400 (16.8)	1,870 (12.8)	8,000 (55.1)	2.8/1	3.6/1
3. Low Bending High Torsion High Axial	Flex Beam Outboard Station	6,800 (46.8)	2,440 (16.8)	1,870 (12.8)	16,000 (110.3)	2.8/1	3.6/1

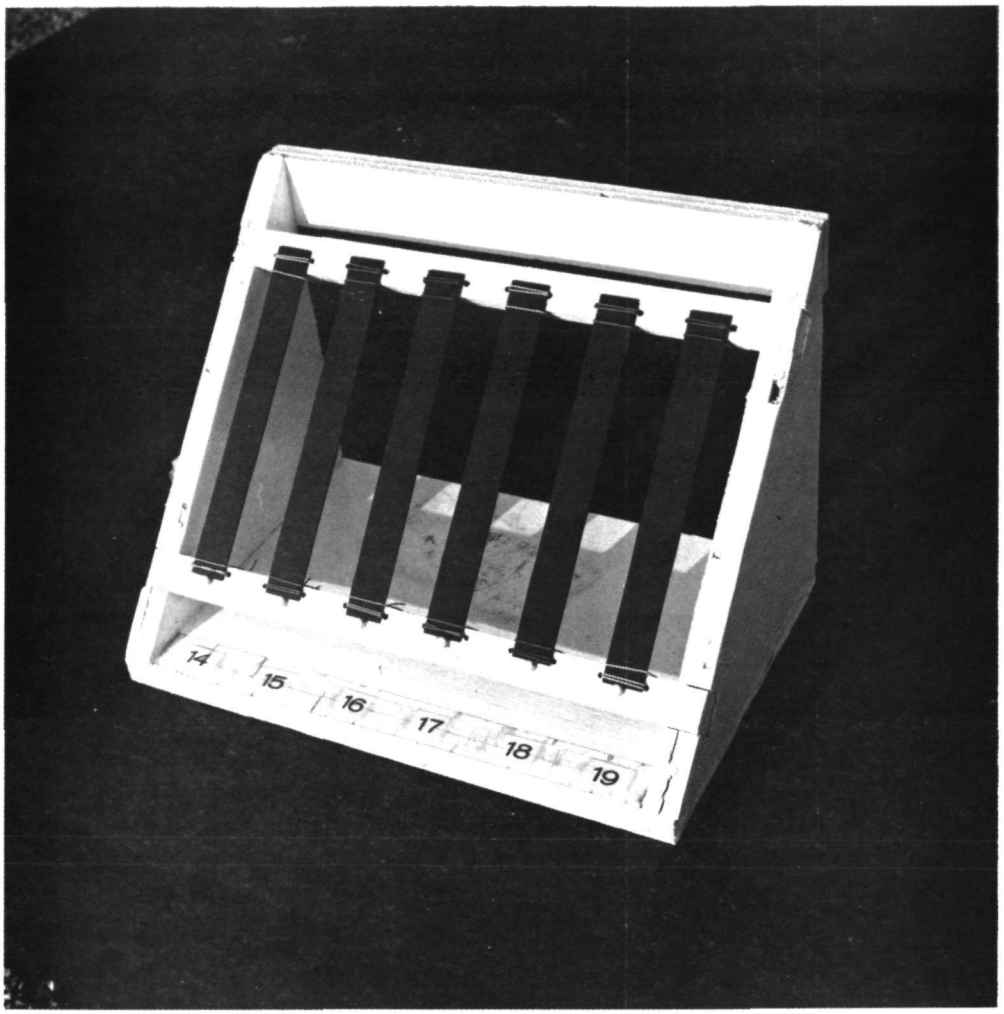

FIGURE 8. SPECIMENS SUBJECTED TO WEATHERING EXPOSURE ON ROOF OF S.A. PLANT.

SECTION 3.0 RESULTS AND DISCUSSION

3.1 COMBINED LOAD FATIGUE TESTS

The actual test stress levels used for each load condition as well as the resulting changes in torsional and flexural moduli are given in Table III. A plot of retained torsional modulus as a function of vibratory torsional stress at 10^7 cycles is shown in Figure 9. Figure 10 shows a plot of retained torsional modulus as a function of vibratory flatwise bending stress at 10^7 cycles. The data points in Figures 9 and 10 represent the results of the individual tests for each load condition. The line drawn through each set of data points represents the best linear least squares fit to the particular set of data points.

As expected, increased vibratory stresses, both torsional and bending, resulted in greater damage as determined by greater changes in torsional modulus. No differences in fatigue vibratory damage was evident due to the 100 percent increase in axial stress from 8000 psi (55.2×10^6 n/m^2) for Condition 2 to 16,000 psi (110.3×10^6 n/m^2) for Condition 3. Thus, torsional and flexural stresses have been shown to have a greater influence on fatigue strength than steady axial stress.

In no case did a specimen show zero damage upon calibration after accumulation of fatigue cycles. This is true even for the lowest stress levels tested, see Table III, and calibration at 10^6 cycles, the lowest cycle level at which recalibration was performed. A check for systematic error in the calibration technique showed that errors in the measurement method are random and much smaller in magnitude than the calculated reductions in modulus. Thus the indicated reductions in modulus are real and not an apparent phenomenon brought about by systematic error in the measuring method. There is some evidence that fiber composites lose a certain amount of their modulus during the first few cycles of a fatigue test due to the fracture of weak fibers. This is an area which could be potentially important and consequently should be the subject of further study.

The torsional modulus change was chosen as the dependent variable in Figures 9 and 10 because torsional modulus decreased to a much greater extent as a function of accumulated fatigue cycles than flexural modulus. A failure criterion of 50 percent reduction in modulus was adopted based on contract requirements even though actual design requirements would dictate smaller reductions in modulus as a failure criterion.

TABLE III

TEST STRESSES AND MODULUS REDUCTION DATA

Specimen Number	Load Condition*	Percent of Flight Stress	Torsional Stress ±PSI ±($n/m^2 x 10^6$)	Flatwise Bending Stress ±PSI ±($n/m^2 x 10^6$)	Edgewise Bending Stress ±PSI ±($n/m^2 x 10^6$)	Initial Modulus $x10^6$ PSI ($x10^9$ n/m^2)		Modulus Reduction at Cycles (Percent)					
								10^6		$5x10^6$		10^7	
						Tors.	Flex	Tors.	Flex.	Tors.	Flex.	Tors.	Flex.
04	1	220	2420 (16.8)	37500 (258.5)	11600 (79.9)	0.78 (5.3)	14.20 (97.8)	4.7	2.0	10.8	2.6	10.8	5.7
06	1	300	3300 (22.7)	51000 (351.5)	15100 (104.0)	0.78 (5.3)	13.33 (91.8)	8.2	2.5	11.9	2.7	12.0	5.0
08	1	350	3850 (26.5)	59500 (410.1)	19200 (132.3)	0.74 (5.1)	13.30 (91.6)	5.1	0.0	9.6	1.2	43.8	6.5
03	1	440	4850 (33.4)	25000 (172.3)	22300 (153.7)	0.72 (4.9)	12.99 (89.5)	18.5	4.0	30.7	17.6	70.0	19.3
09	2	220	3510 (24.1)	15000 (103.4)	5380 (137.0)	0.72 (4.9)	13.70 (94.4)	5.8	0.5	7.8	1.0	7.4	0.5
05	2	300	5610 (38.6)	20400 (140.6)	8080 (55.7)	0.74 (5.1)	13.36 (92.1)	7.2	1.0	5.6	1.9	5.9	2.9
07	2	350	6540 (45.0)	23800 (164.0)	8540 (58.8)	0.73 (5.0)	14.06 (96.9)	7.4	1.5	38.5	3.4	56.2	3.9
01	2	400	7480 (51.5)	27200 (187.5)	10900 (75.1)	0.72 (4.9)	13.56 (93.4)	8.5	3.1	29.7	4.1	73.6	5.1
11	3	220	3510 (24.1)	15000 (103.4)	5330 (36.7)	0.78 (5.3)	12.72 (87.6)	3.0	0.0	0.0	2.9	3.5	2.6
10	3	300	5610 (38.6)	20400 (140.6)	7750 (53.4)	0.72 (4.9)	13.72 (94.5)	9.2	0.0	11.5	2.5	12.6	3.0
02	3	350	6540 (45.0)	23800 (164.0)	9050 (62.3)	0.75 (5.1)	13.52 (93.2)	12.8	2.4	39.5	3.3	45.2	2.4
12	3	400	7480 (51.5)	27200 (187.5)	10300 (71.0)	0.73 (5.0)	13.28 (91.5)	13.3	0.4	17.3	0.4	50.0	0.4

*For Load Condition 1 Axial Stress = 4000 PSI (27,596) n/m^2

For Load Condition 2 Axial Stress = 8000 PSI (55,152) n/m^2

For Load Condition 3 Axial Stress = 16000 PSI (110,304) n/m^2

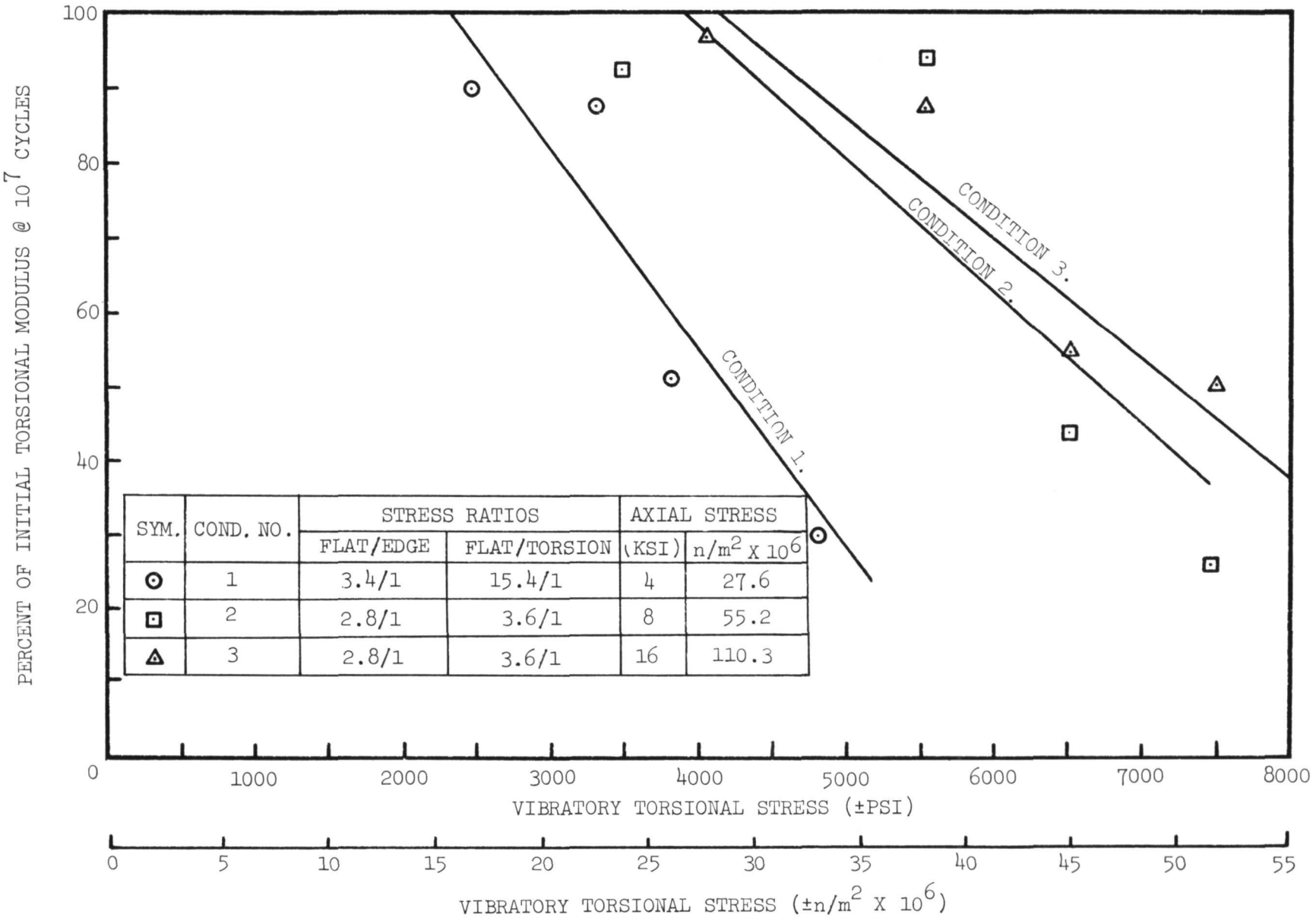

SYM.	COND. NO.	STRESS RATIOS		AXIAL STRESS	
		FLAT/EDGE	FLAT/TORSION	(KSI)	n/m^2 X 10^6
⊙	1	3.4/1	15.4/1	4	27.6
⊡	2	2.8/1	3.6/1	8	55.2
△	3	2.8/1	3.6/1	16	110.3

FIGURE 9. SIGNIFICANT MODULUS REDUCTION EXPERIENCED WITH INCREASED TORSIONAL STRESSES.

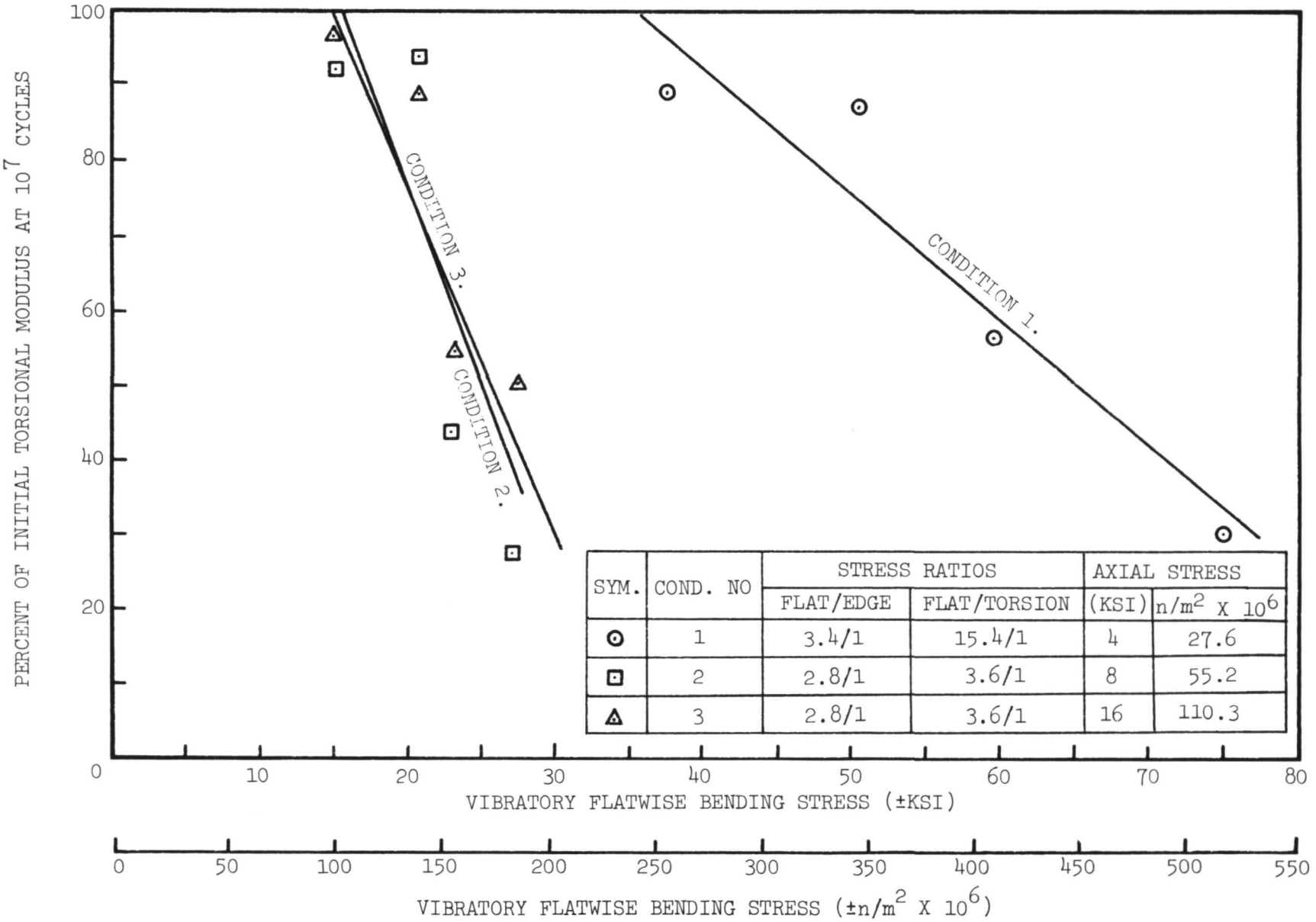

FIGURE 10. SIGNIFICANT MODULUS REDUCTION EXPERIENCED WITH INCREASED BENDING STRESS.

The values of torsional and bending stresses which give a 50 percent reduction in torsional modulus are plotted in a constant life diagram in Figure 11 and are extrapolated from the data presented in Table III.

The data points for the 10^7 cycle line in Figure 11 were taken from Figures 9 and 10. The points for the 5×10^6 cycles line had to be extrapolated about 10 percent from the data of Table III. A small linear extrapolation like this is considered valid. For this reason we have good confidence in the 5×10^6 and 10^7 cycles lines shown in Figure 11. However, the data points shown for the 10^6 cycles line were obtained by extrapolating the data in Table III by more than 30 percent. Therefore, the confidence level for the 10^6 cycles data is much lower and this curve is shown in phantom in Figure 11. The data of Table III could be used to make constant life diagrams for modulus reductions other than 50 percent. This would generate a family of curves similar to those shown in Figure 11 which could be used for design purposes. Further combined load tests as well as torsion only and bending only fatigue tests should be conducted not only to increase the range of load conditions over which the lines of Figure 11 extend but also to substantiate the results of the present investigation. This additional substantiation is needed because the lines plotted in Figure 11, for any of the constant cycle curves, contains data for two different flatwise to edgewise stress ratios and three different axial stresses.

As a result of this test program we have been able to establish preliminary curves for the interaction of bending and torsional stresses which will produce a specified amount of modulus reduction. Such information will help the designer determine the actual blade geometry in a manner that will enable such blades to operate within safe load levels for the design life of the blade.

3.2 DAMPING AND NATURAL FREQUENCY MEASUREMENTS

The damping and natural frequency measurements obtained for all specimens are given in Table IV. Values of the percentage change of C/C_c, the ratio of damping capacity to critical damping capacity, and f, the natural frequency, are also given in Table IV. A comparison of percent change in C/C_c as a function of percent change in torsional modulus, Figure 12, shows that there is very little change in C/C_c except in those specimens which show fairly large changes in torsional modulus, at least 30 percent. This is due to the fact that the specimens with large changes in torsional modulus exhibited cracks along the scrim ply at the center of the thickness direction. This cracking in the more highly stressed

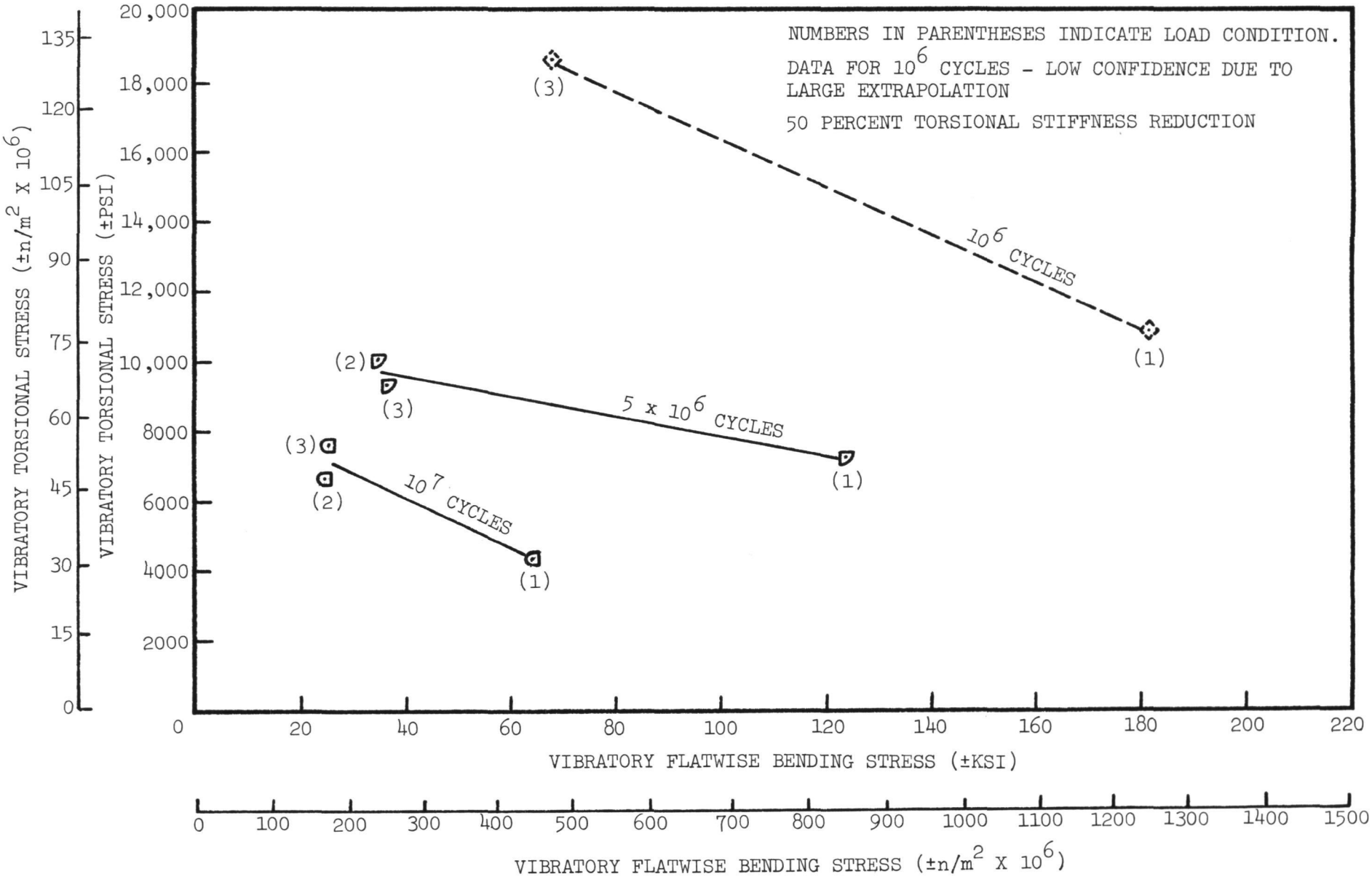

FIGURE 11. CONSTANT-LIFE DIAGRAM PROVIDES COMBINED LOAD DESIGN DATA.

TABLE IV

DAMPING AND NATURAL FREQUENCY MEASUREMENTS AS A FUNCTION OF FATIGUE CYCLES

Specimen Number	Load Cond.	Percent of Flight Stress	C/C_c and Frequency, at Cycles								Percent Change of C/C_c and Frequency Compared to 0 Cycle Values, at Cycles					
			0		10^6		$5x10^6$		10^7		10^6		$5x10^6$		10^7	
			C/C_c $x10^{-3}$	Freq Hz	C/C_c $x10^{-3}$	Freq Hz	C/C_c $x10^{-3}$	Freq Hz	C/C_c $x10^{-3}$	Freq Hz	C/C_c	Freq	C/C_c	Freq	C/C_c	Freq
04	1	220	12.6	6.67	21.9	6.23	20.9	6.40	20.7	6.32	+73.8	-6.6	+65.9	-4.1	+64.3	-5.2
06	1	300	12.1	6.41	—	—	20.8	6.00	13.1	6.35	—	—	+71.9	-6.4	+8.3	-1.0
08	1	350	9.8	6.85	10.0	6.81	9.5	6.87	25.82	6.66	+2.0	-0.6	-3.1	+0.3	+163.5	-2.8
03	1	440	19.2	6.15	34.5	5.86	117.0	5.48	181.0	5.11	+79.7	-4.7	+509.4	-10.9	+842.7	-16.9
09	2	220	10.3	7.06	9.25	7.12	7.44	7.09	7.44	7.09	-10.2	+0.8	-27.8	+0.4	-27.8	+0.4
05	2	300	11.0	6.94	11.2	6.94	—	—	9.75	7.02	+1.8	0.0	—	—	-11.4	+1.2
07	2	350	9.0	7.06	8.0	7.09	13.7	7.02	15.3	6.94	-11.1	+0.4	+52.2	-0.6	+70.0	-1.7
01	2	400	13.3	7.19	15.3	7.18	15.5	7.29	20.7	7.11	+15.0	-0.1	+16.5	+1.4	+55.6	-1.1
11	3	220	5.5	5.71	7.4	5.69	7.4	5.71	7.2	5.69	+34.5	-0.4	+34.5	0.0	+30.9	-0.4
10	3	300	13.1	6.63	11.7	6.53	11.2	6.51	11.9	6.51	-10.7	-1.5	-14.5	-1.2	-9.2	-1.2
02	3	350	6.4	6.52	9.8	6.46	12.8	6.41	16.1	6.38	+53.1	-0.9	+100.0	-1.7	+151.6	-2.1
12	3	400	6.1	6.42	9.3	6.45	9.8	6.37	11.7	6.37	+52.5	+0.5	+60.7	-0.8	+91.8	-0.8

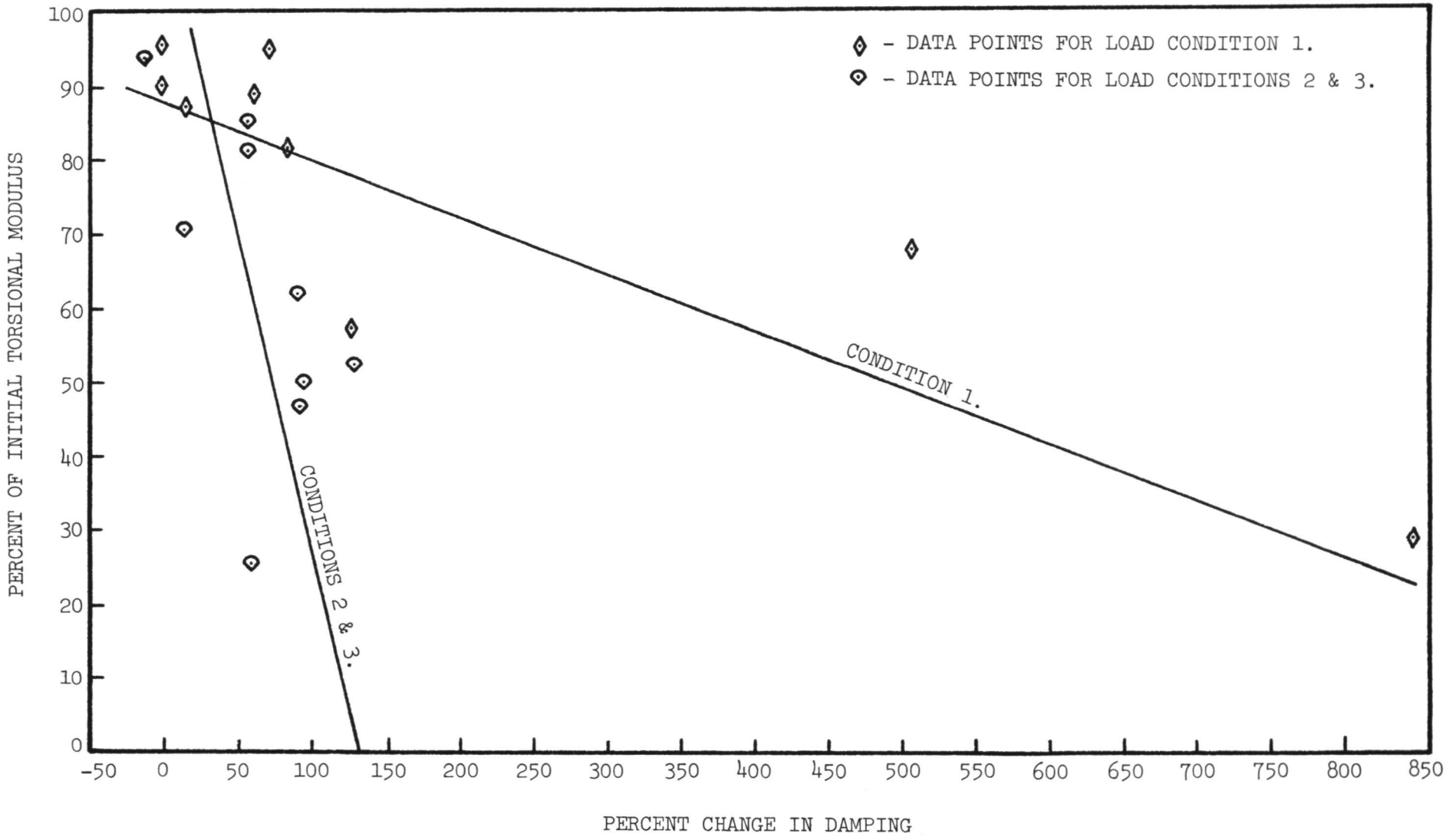

FIGURE 12. SIGNIFICANT DAMPING CHANGES OCCUR ONLY AFTER LARGE CHANGES IN MODULUS, INDICATING SIGNIFICANT DAMAGE.

specimens will be discussed in more detail in the following section. Because of the small and somewhat random nature of the change in C/C_C, damping measurements as performed in this investigation are not considered a sufficiently sensitive means of detecting small amounts of damage in these composite specimens.

3.3 FAILURE ANALYSIS

Although no specimen exhibited catastrophic failure, microscopic investigation shows that the dominant failure mode for all test conditions was cracking in the resin rich, scrim layer between graphite plies. Such cracks were observed only in those specimens which were tested at 3.5 or more time flight stresses, thus cracks were observed only in those specimens which had a reduction in torsional modulus of 30 percent or more. In addition to the cracks parallel to the scrim plies, the most highly stressed Condition 1 specimen, 4.4 times flight stresses, also cracked perpendicular to the scrim plies, that is through the graphite layers. Such cracks ran from the centerline (scrim ply) crack across the graphite plies to the surface. These cracks only appeared in those specimens which had a torsional modulus reduction of more than about 50 percent.

Figure 13 illustrates the typical cross section of an undamaged specimen. A centerline crack typical of those observed in the highly stressed specimens is shown in Figure 14. These cracks originated at the end of the specimen which was subjected to the highest bending stress. They traveled in both directions from the end of the fiberglass doubler, see Figure 2. In the direction toward the doubler, cracks were observed as far as the first bolt hole, about one-quarter of an inch (.64 cm) from the end of the doubler. In the other direction, along the gauge length, cracks were observed from one-third to one-half of the specimen gauge length, from two to three inches (5.1 - 7.6 cm).

Figure 15 shows the cracks which run between the centerline crack and the specimen surface on the most highly stressed specimens. Failure or cracks in the thickness direction, as shown in Figure 15, is the expected failure mode resulting from torsion since in torsion testing of homogeneous rectangular beams the maximum shear stress occurs in the center of the wide face. The fact that the primary failure mode was cracking along the resin rich area of the scrim ply where stresses are below maximum indicates that the scrim ply or perhaps the resin rich area alone may be creating a plane of inherent weakness. Such a plane of weakness may permit crack initiation and propagation to occur more readily than in the plane of maximum stress. The effect of the scrim ply and/or resin thickness between graphite plies in creating centerline cracks is an area which deserves further study.

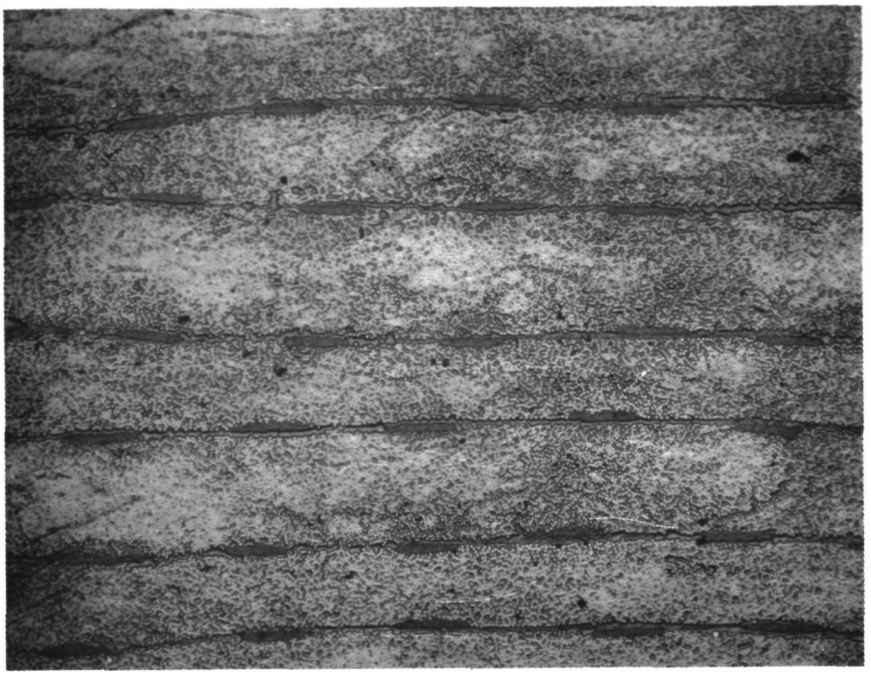

FIGURE 13. TYPICAL UNDAMAGED CROSS SECTION - 50x MAGNIFICATION.

FIGURE 14. TYPICAL CENTERLINE CRACK IN RESIN RICH SCRIM AREA 50x MAGNIFICATION.

FIGURE 15. TYPICAL CENTERLINE CRACK SHOWN INTERSECTING CENTERLINE SCRIM PLY CRACK. 50x MAGNIFICATION.

3.4 NATURAL AND ARTIFICIAL WEATHERING

"As fabricated", and "as aged", weights and dimensions of the natural and artificial weathered specimens are given in Table V. The as weathered weights of specimens were taken at two times, within 24 hours of removal from the weathering installation and again after one week from the time the specimens were removed from the weathering installation. Examination of these weights indicate that the natural weathering specimens absorbed a small amount of moisture, about one-tenth of one percent by weight, during the 143 days of exposure. Approximately half of this moisture was lost during one week in the laboratory. The natural weathering specimens showed no significant changes in specimen dimensions.

The artificial weathering specimens exhibited a slight weight loss, about one-half of one percent, when weighed within 24 hours after exposure of 600 hours on each face. One week later the weight loss was greater, indicating some loss of moisture. As with the natural weathering specimens, the moisture content was about one-tenth of one percent by weight.

Photographs of the surface condition of the virgin, naturally, and artificially weathered specimens are shown in Figure 16. Figure 16 shows how the resin has been leached away from the scrim ply side of the specimen in the artificial weathering specimen, thus making the scrim clearly visible. Associated with the resin loss is a reduction of about 0.002 inches (.051 mm) in the thickness of the artificial weathering specimens. Except for slight staining no other surfaces of any of the weathering specimens seem to have been effected by the exposure. A small, but not visible, amount of resin removal on all specimens has likely taken place.

The woven scrim fabric, seen clearly on the surface of the artificially weathered specimen in Figure 16, was not applied properly by the prepreger. The scrim should have a 0^{o}, 90^{o} orientation instead of the 0^{o}, 60^{o} orientation shown. This misorientation is probably due to a slight bias tension applied to the scrim during the prepreging operation. Comparison of the mechanical properties, including torsional modulus, of the specimens tested in this study with specimens made from similar material but with the scrim properly oriented show that the effect of misoriented scrim on such properties is negligible.

TABLE V

WEIGHTS AND DIMENSIONS OF WEATHERING SPECIMENS AS FABRICATED AND AFTER WEATHERING

Specimen Number	As Fabricated			As Aged				Change in Weight Percent	
	Width Inches (cm.)	Thickness Inches (cm.)	Weight Grams	Weight Inches (cm.)	Thickness Inches (cm.)	Weight, 24 Hrs* Grams	Weight, 1 Wk+ Grams	24 hr	1 wk
				NATURAL WEATHERED SPECIMENS					
14	1.020 (2.59)	0.095 (0.21)	21.9069	1.019 (2.59)	0.094 (.239)	21.9393	21.9292	+0.2	+0.1
15	1.026 (2.61)	0.106 (.269)	24.2774	1.026 (2.61)	0.105 (.267)	24.3165	24.3041	+0.2	+0.1
16	1.007 (2.56)	0.109 (.277)	24.9511	1.008 (2.56)	0.109 (.277)	24.9850	24.9746	+0.1	+0.1
17	1.023 (2.60)	0.102 (.259)	23.7168	1.023 (2.60)	0.102 (.259)	23.7595	23.7468	+0.2	+0.1
18	1.026 (2.61)	0.104 (.264)	24.1245	1.026 (2.61)	0.104 (.264)	24.1597	24.1487	+0.1	+0.1
19	1.024 (2.60)	0.106 (.269)	24.6948	1.029 (2.61)	0.106 (.269)	24.7289	24.7191	+0.1	+0.1
				ARTIFICIAL WEATHERED SPECIMENS					
20	1.023 (2.60)	0.102 (.259)	23.0852	1.025 (2.60)	0.099 (.251)	23.0065	22.9717	-0.3	-0.5
21	1.030 (2.62)	0.101 (.256)	23.5849	1.030 (2.62)	0.099 (.251)	23.4312	23.3961	-0.7	-0.8
22	1.019 (2.59)	0.106 (.269)	24.4018	1.025 (2.60)	0.104 (2.64)	24.3129	24.2847	-0.4	-0.5
23	1.034 (2.63)	0.099 (.251)	23.1260	1.038 (2.64)	0.097 (.246)	23.0156	22.9941	-0.5	-0.6
24	1.016 (2.58)	0.096 (.244)	21.8168	1.021 (2.59)	0.093 (.236)	21.7611	21.7224	-0.3	-0.4
25	1.034 (2.63)	0.096 (.244)	22.4703	1.035 (2.63)	0.095 (.241)	22.3084	22.2900	-0.7	-0.8

*Weights measured within 24 hours of removal from test facility

+Weights measured after one week of removal from test facility

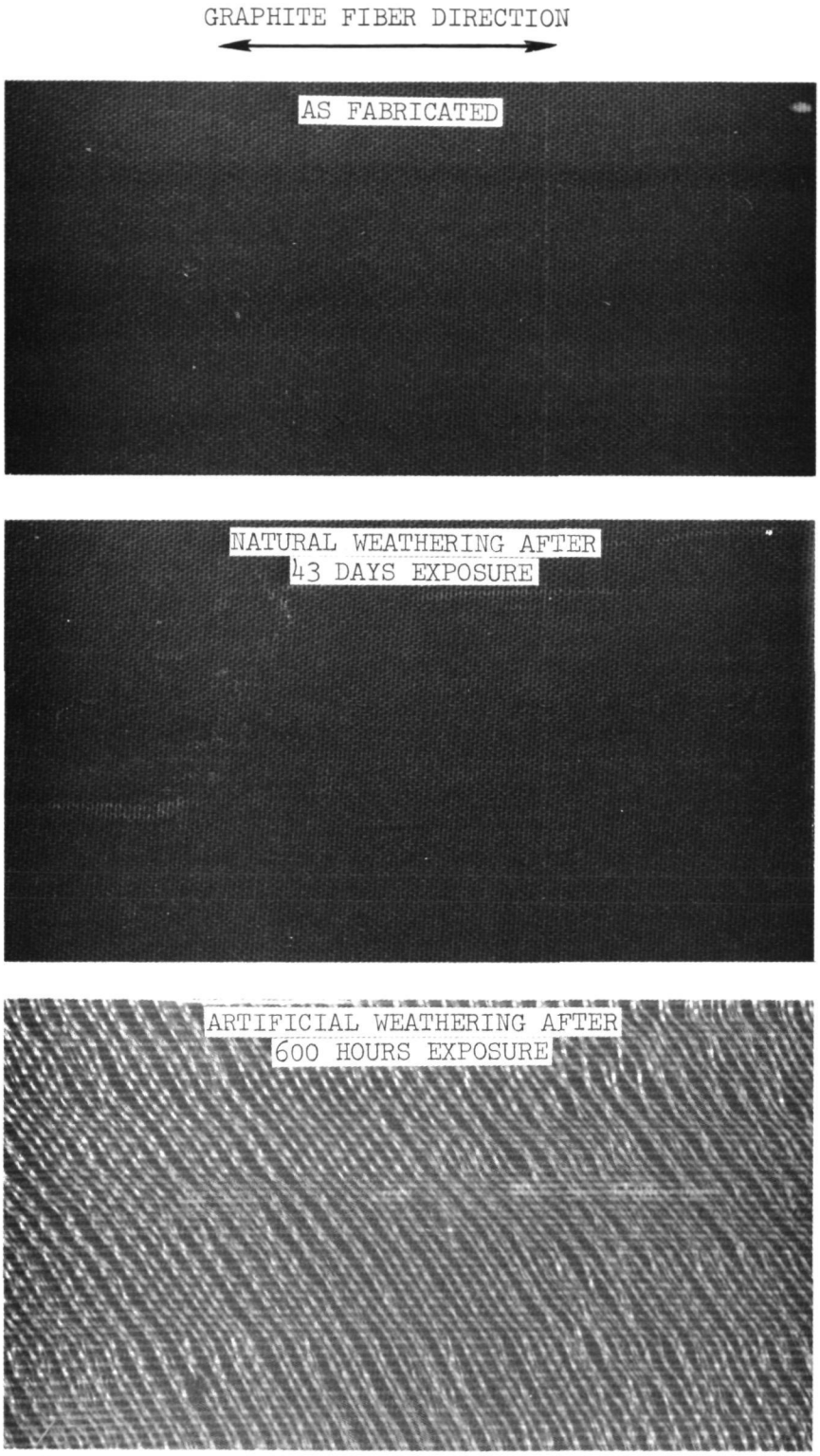

FIGURE 16. ARTIFICIAL WEATHERING MORE SEVERE THAN NATURAL WEATHERING. ALL PHOTOGRAPHS 3x MAGNIFICATION.

SECTION 4.0 CONCLUSIONS

1. For stress levels up to three times predicted flight stresses, combined load fatigue testing produced fatigue damage resulting in a reduction of torsional modulus of less than 15 percent and a reduction in flexural modulus of less than 6 percent at 10^7 cycles.

2. Stress levels from 3.5 to 4.4 times predicted flight stresses resulted in matrix cracking and reductions of torsional modulus of 45 to 75 percent as well as reduction of flexural modulus up to 20 percent at 10^7 cycles.

3. Fatigue testing for 10^7 cycles at the highest stress levels did not result in fracture.

4. For a given percentage of torsional modulus reduction (50 percent in this case) a relationship has been established between torsional and flexural stresses. Such a relationship can be used as a design guide to predict combined load levels which will give a desired fatigue life.

5. The effect of steady axial stress in the range of 4000 psi (27.6×10^6 n/m^2) to 16,000 psi (110.3×10^6 n/m^2) has very little effect on the combined load fatigue strength of the graphite-glass scrim-epoxy specimens tested in this study.

6. The ratio of damping capacity to critical damping capacity, C/C_c, increases significantly from the value for the virgin specimen only for those specimens subjected to high stresses, 3.5 to 4.4 times flight stresses. This is the same stress range which produces centerline cracks in the test specimens as a result of fatigue cycling. The large changes in damping are directly related to the cracking of the specimen. Changes in damping do not appear to be a very sensitive measurement of small amounts of damage in fiber composite materials.

7. Weathering tests show that completely unprotected graphite-glass scrim-epoxy materials absorb slight amounts (less than 1 percent by weight) of moisture when subjected to either natural or artificial weathering. Artificial weathering is capable of leaching or dissolving the Dexter Materials Corp. DM-101 resin with which the present specimens were prepreged. Less than one percent of the total specimen weight was lost as a result of resin leaching. It must be assumed that prolonged periods of natural weathering would also remove some of this resin. The effects of any type of protective coating have not been evaluated.

SECTION 5.0 RECOMMENDATIONS FOR FURTHER STUDIES

1. Those specimens subjected to natural and artificial weathering should be fatigue tested in the combined load machine to determine the effect of environmental exposure on the fatigue strength of graphite-glass scrim-epoxy composites.

2. The range of torsional and bending fatigue stresses used for combined load fatigue testing should be expanded to give as broad a range as possible for the constant life data generated in this test program.

3. The effect of the first few fatigue cycles on the torsional and flexural modulus of fiber composite materials should be evaluated in detail. If, as has been suggested, the first few fatigue cycles breaks weak fibers thus lowering either the load carrying capacity or the modulus or both of a composite part then such parts should be designed to the lower material values. A means of accurately determining such lower values should be established.

4. The effect of the scrim ply and/or resin rich area between graphite plies in creating a plane of inherent weakness in built up fiber composite structures subjected to combined torsional and flexural loading should be evaluated. If such a plane of weakness can be eliminated by changes in layup technique then a greater proportion of the composite materials theoretical strength should be able to be utilized.

SECTION 6.0 REFERENCES

(a) NASA Contract No. NAS1-10960, Bearingless Helicopter Rotor Concept Having a Carbon Fiber-Epoxy Primary Structure, work performed by United Aircraft Research Laboratories by M. C. Cheney.

(b) Sikorsky Standard SS9611, Graphite Fiber/Resin Matrix Preimpregnated Materials for Structural Composites, dated June 5, 1973.

NASA Scientific & Technical Information Facility
Attn: Acquisitions Branch
P. O. Box 33
College Park, MD 20740